Review in Advance first posted online on July 31, 2013. (Changes may still occur before final publication online and in print.)

Turbulence in the Upper-Ocean Mixed Layer

Eric A. D'Asaro

Applied Physics Laboratory and School of Oceanography, University of Washington, Seattle, Washington 98105; email: dasaro@apl.washington.edu

Annu. Rev. Mar. Sci. 2014. 6:4.1–4.15

The *Annual Review of Marine Science* is online at marine.annualreviews.org

This article's doi: 10.1146/annurev-marine-010213-135138

Keywords

mixing, waves, Langmuir circulations

Abstract

Nearly all operational models of upper-ocean mixing assume that the turbulence responsible for this mixing is driven by the atmospheric fluxes of momentum, heat, and moisture and the shear imposed by the ocean circulation. This idealization is supported by historical measurements of dissipation rate within the boundary layer. Detailed measurements made recently by many investigators and supported by theoretical and numerical results have found significant deviations from this classical view attributable to the influence of surface waves. Although a review of these measurements finds strong support for the influence of waves—and, in particular, for the predictions of large-eddy simulations, including the Craik-Leibovich vortex force—there are insufficient data to give definitive support to a new paradigm.

1. INTRODUCTION

The upper boundary layer of the ocean figures prominently in the global climate system because it mediates momentum, heat, and gas fluxes between the ocean and the atmosphere. Ultimately, these fluxes are governed by the dynamics of turbulent vertical mixing in this boundary layer. Current climate models typically have large errors in boundary-layer thickness (e.g., **Figure 1**) (Belcher et al. 2012, Fox-Kemper et al. 2011), with similar errors extending across the entire range of ventilated water masses originating in the mixed layer (Sallée et al. 2013a,b). Although many factors can contribute to these errors, one obvious candidate is the parameterization of mixing in the upper-ocean boundary layer. A variety of such parameterizations exist, but they all rely on basic physical assumptions about the factors that govern the mixing rates. This article addresses the question of whether these assumptions are correct by reviewing measurements of turbulence in the upper-ocean boundary layer in the context of existing and proposed models of this turbulence.

2. THE CLASSICAL APPROACH

The current-generation upper-ocean mixing parameterizations use the air–sea fluxes of momentum, heat, and moisture and the subsurface profiles of shear and stability to predict the profiles of turbulent vertical eddy fluxes. The divergence of these fluxes then defines the effect of the mixing. A collection of these models has recently been gathered together with a uniform software structure under the General Ocean Turbulence Model project (Umlauf & Burchard 2005). The structure of these models draws heavily on the vast literature describing laboratory turbulent flows and on measurements of atmospheric boundary layers, thereby compensating for the limited ocean observations. However, the ocean surface is not a solid boundary, as the boundaries of terrestrial atmospheric or classical laboratory flows are. Instead, as every sailor knows, it is constantly in motion owing to the action of surface waves. The classical approach ignores these waves; this review focuses on whether this neglect is justified experimentally.

3. MEASUREMENT CHALLENGES

Progress in properly modeling upper-ocean turbulence has been limited by the difficulty of making detailed turbulence measurements in this region. At a minimum, vertical profiles of mean temperature $\langle\theta\rangle(z)$, salinity $\langle S\rangle(z)$, and velocity $\langle\mathbf{u}\rangle(z)$; the associated turbulent fluxes $\langle\theta' w'\rangle$, $\langle S' w'\rangle$,

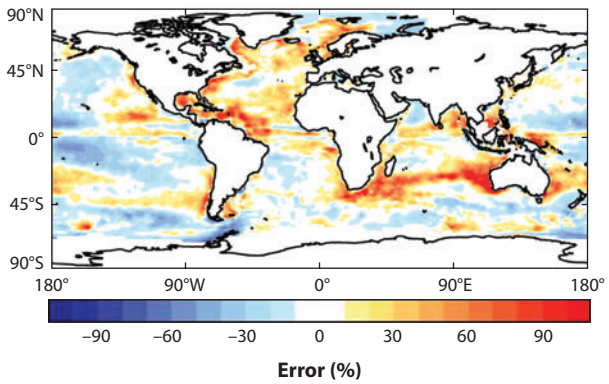

Figure 1

Errors in mixed-layer depth in June, July, and August from the HadGEM3 climate model. Adapted from Belcher et al. (2012).

$\langle v'w' \rangle$, and $\langle u'w' \rangle$; the variances $\langle \theta'^2 \rangle$, $\langle u'^2 \rangle$, $\langle v'^2 \rangle$, and $\langle w'^2 \rangle$; and the rates of dissipation of variance of kinetic energy ε, temperature χ, and salinity χ_S would provide a basic data set for model verification. Here, $\langle X \rangle$ implies an appropriate time and/or space average to isolate the turbulent component of variable X, and $X' = X - \langle X \rangle$.

Only a small fraction of this set of measurements can be made in the ocean with available instruments and sensors. One major difficulty is isolating the small turbulent signal in the face of much larger nonturbulent motions. Typical turbulent velocities of 0.01 m s^{-1} have spatial scales ranging from centimeters to a few times the mixed-layer depth of 10 m to hundreds of meters. These are superimposed on oscillating surface wave velocities on the order of 1 m s^{-1} with periods of 1–10 s and wavelengths of meters to hundreds of meters. The surface wave signal decays with depth, but the decay scale of the longer waves is comparable to the mixed-layer depth, so these are present across the entire layer. High-frequency fluctuations in the ocean interior are dominated by internal gravity waves (Munk 1981) and have a broad range of frequencies, from the inertial period (~24 h at 30°N) to the buoyancy period (typically 500 s in the upper ocean, with a broad range of lateral wavelengths, from tens of meters to hundreds of kilometers). Although these waves cannot propagate vertically within the upper mixed layers, their horizontal velocities in the mixed layer are similar to those immediately below (D'Asaro 1978), typically 0.05 m s^{-1}, and are much larger during periods of strong inertial frequency forcing (Pollard & Millard 1970). More important, the horizontal wavenumber spectrum of internal waves, roughly -2, is similar to the $-5/3$ expected of turbulence. Thus, the turbulent motions are not easily separated from surface and internal wave motions with comparable time and space scales and much larger amplitudes. For example, a velocity sensor with a linearity of 1% operating in a typical surface wave field generates nonlinear noise of the same amplitude as the turbulence signal. Similarly, the velocities of a ship or other platform floating on the surface waves are much larger than the turbulent velocities, making it difficult to take turbulence measurements directly from these platforms.

One successful approach has been to focus on the smallest scales, where turbulence dominates, and to estimate the dissipation rates of energy ε and temperature χ [the salinity dissipation rate χ_S remains largely unmeasured owing to its very small (millimeter) scales]. Traditional microstructure techniques using fast-response sensors on vertical or horizontal profiling instruments (Gregg 1998) are effective, as are acoustic Doppler and other specialized sensors (Thomson et al. 2009), particularly when mounted on surface-following platforms to minimize the surface wave effects.

In shallow water, the ocean bottom provides a highly stable reference for instrumentation platforms. Arrays of fixed sensors spanning the mixed layer (Gerbi et al. 2009) or multibeam acoustic Doppler current profilers (Gargett & Wells 2007) can measure many of the needed turbulent variances and covariances, particularly if a large number of beams are used (Vermeulen et al. 2011). However, the boundary-layer turbulence in shallow water may differ from that in the open ocean, because the surface waves are significantly modified by bottom interactions and because near-bottom velocities driven by surface waves, tides, and lower-frequency flows can generate strong bottom-generated turbulence not present in the open ocean.

The research platform FLIP (Floating Instrument Platform), a 108-m-long manned spar buoy, provides a stable platform for detailed upper-ocean and lower-atmosphere measurements. Clouds of bubbles created by breaking surface waves in the upper few meters of the ocean reflect sound strongly. Multiple horizontally directed and scanning sonars mounted on FLIP have been successful in measuring the spatial structure and horizontal velocities of these bubble clouds (Smith 1989, 1992) and thus also the near-surface turbulent velocity variations $\langle v'^2 \rangle$ and their horizontal variations. Surface waves can be removed successfully or measured by spatial and temporal averaging. However, the strong backscatter from these same bubbles makes it difficult to measure the

subsurface velocities using similar sonars. Upward-looking sonars made from stable unmanned platforms (Zedel & Farmer 1991) have measured the vertical distribution of bubbles, and current meters deployed from FLIP have measured all three components of velocity (Weller & Price 1988). Neither technique, however, has produced useful measures of velocity variances or covariances away from the surface.

Neutrally buoyant Lagrangian floats (D'Asaro 2003, D'Asaro et al. 1996) can measure vertical velocity w, its variance $\langle w'^2 \rangle$, and the associated scalar fluxes $\langle \theta' w' \rangle$ and $\langle S' w' \rangle$ (D'Asaro 2001, 2004) as well as associated spectra and cospectra across the entire mixed layer. The velocity is measured from the motion of these floats as they are repeatedly carried across the mixed layer by the turbulence. Surface waves are filtered from the vertical velocity by measuring the float's depth using pressure; the waves have no pressure signal along particle trajectories. Horizontal velocities can be measured by tracking the floats acoustically, but the similarity of the turbulent and internal wave spectra makes it difficult to isolate the turbulent component or measure the horizontal velocity covariances. Detailed published analyses exist only for $\langle w'^2 \rangle$ and its depth dependence and frequency spectra.

In summary, direct measurements of surface mixed-layer turbulence in the open ocean are limited to the dissipations ε and χ and the variances $\langle \theta'^2 \rangle$, $\langle u'^2 \rangle$, $\langle v'^2 \rangle$, and $\langle w'^2 \rangle$, with the horizontal components measured only at the surface. More detailed analyses exist for shallow water.

4. SUPPORT FOR THE CLASSICAL APPROACH

Kinetic energy dissipation measurements have generally supported the classical model. There are two limiting cases. First, for weak winds and strong air–sea heat fluxes, the turbulence scales with the surface flux of buoyancy $J_b = g/\rho[\frac{\alpha}{C_P} Q_s + \beta \frac{S}{1-S} L Q_l]$, where g is the acceleration of gravity, ρ is the density of seawater, α is the thermal expansion coefficient, C_P is the specific heat of seawater, β is the haline contraction coefficient, S is the salinity, and Q_s and Q_l are the surface sensible and latent heat fluxes, respectively. Under convective conditions—e.g., the atmosphere cooling the ocean—dissipation should scale with $\varepsilon_f = J_b$. Lombardo & Gregg (1989) and Shay & Gregg (1986) reported that ε/J_b is nearly constant with depth z across the entire boundary layer $0 < z < D$. Its average value (**Figure 2*a*,*b***) is nearly identical to that for the atmospheric boundary layer (**Figure 2*c***). Second, for strong winds and weak air–sea buoyancy fluxes, the turbulence classically scales as $\varepsilon_s = u_*^3/kz$ near the surface, where the von Karman constant $k = 0.41$. For this case, Lombardo & Gregg (1989) found that $\varepsilon = 1.76\varepsilon_s$. For mixed cases where both wind and convection are important, they found that the measured dissipation rates are best fit by $\varepsilon = 0.58\varepsilon_f + 1.76\varepsilon_s$, the sum of the convective and shear scaling (**Figure 2*d***) but with an additional factor of 1.76 on ε_s. Carniel et al. (2012) reported that the same expression applies for buoyancy fluxes of both signs. These results support the classical scaling but include the additional multiplier of 1.76, suggesting an additional energy source from wind or waves.

Measurements of kinetic energy produce a similar result. For buoyancy-driven flows, Steffen & D'Asaro (2002) used Lagrangian floats in Labrador Sea deep convection to find a best fit to the measured rms vertical velocity: $\langle w^2 \rangle^{1/2} = 0.66(J_b H)^{1/3} - 0.0047\,\mathrm{m\,s^{-1}}$. The first term is consistent with classical nonrotating scaling; the second suggests additional small unknown processes or errors. In a more detailed comparison with large-eddy simulations (LESs), Harcourt et al. (2002) reported similar agreement, with much of this error occurring in the upper part of the layer, possibly owing to interaction with baroclinic eddies. For strong winds and weak buoyancy fluxes, classical scaling predicts $\langle w^2 \rangle$ scaling with $u_*^2 = \tau/\rho$, where τ is the wind stress. Data from Lagrangian floats show that this scaling holds remarkably well, both on timescales of hours

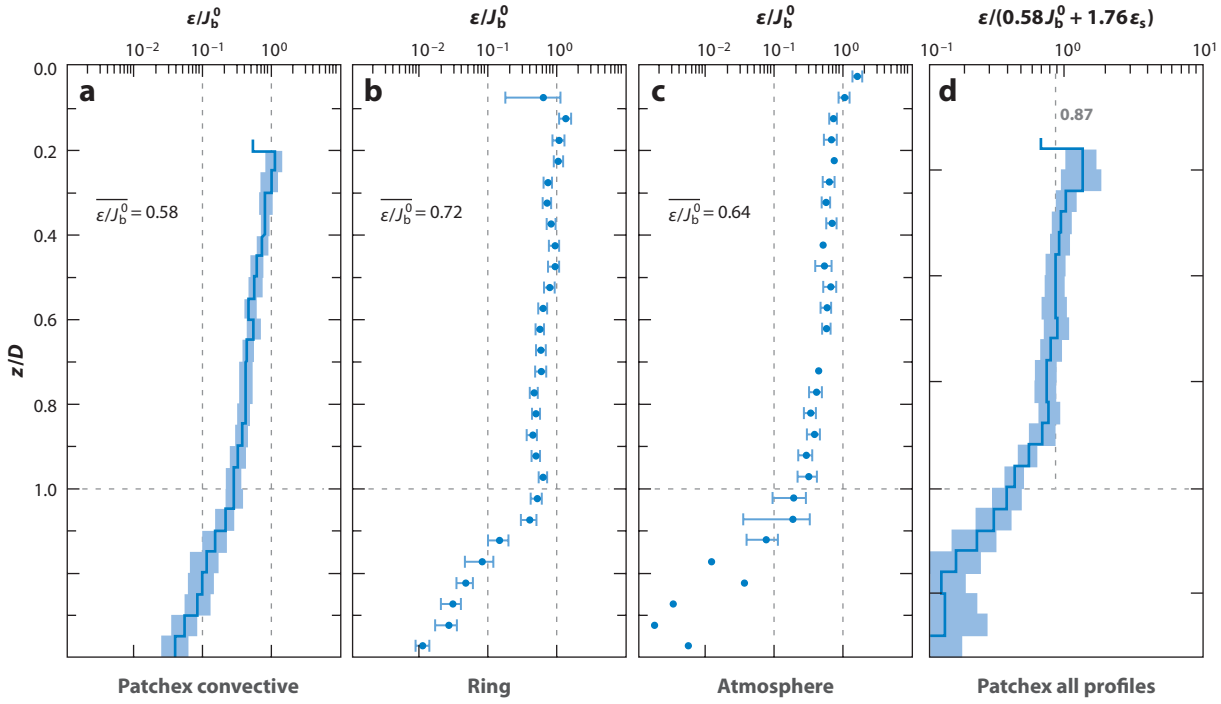

Figure 2

Dissipation rates in the upper-ocean mixed layer scaled by buoyancy flux (panels *a* and *b*) support the classical model of scaling and agree with results from the atmospheric boundary layer (panel *c*). Panel *d* shows the dissipation rates under a combined wind and buoyancy forcing scale with a combination of classical buoyancy and wind scaling; here, the ratio of mixed-layer depth to Monin-Obukov depth ($D/-L$) ranges from 0.4 to 250. Adapted from Lombardo & Gregg (1989).

(**Figure 3*a***) (D'Asaro 2001) and when averaged over an entire deployment (**Figure 3*b***) (Tseng & D'Asaro 2004). However, the value of $\langle w^2 \rangle$ is consistently higher than expected from classical scaling. Laboratory and under-ice boundary layers show $\langle w^2 \rangle / u_*^2 \leq 1$ (Cantwell 1981, McPhee & Smith 1976), with a canonical value of approximately 0.6. In contrast, **Figure 3** shows $\langle w^2 \rangle / u_*^2 \geq 1$. Independent measurements made by Gerbi et al. (2009) using bottom-mounted sensors also show $\langle w^2 \rangle / u_*^2 \geq 1$. As with the dissipation measurements, these results support the classical scaling but include a modest excess in energy, suggesting an additional energy source from wind or waves.

5. WAVES OR WIND?

Surface waves are the most likely source of additional energy for the boundary layer. Surface wave amplitudes, however, are closely correlated with the wind, particularly at the higher frequencies that contribute most to the wave slope and Stokes drift. This is shown by 100 days of waverider buoy data at ocean station Papa (50°N, 145°W, Coastal Data Information Program station 166; **http://cdip.ucsd.edu**). The increasingly tight relationships between wind speed and significant wave height (**Figure 4*a***), wind stress and surface Stokes drift (**Figure 4*b***), and wind stress and wave slope (**Figure 4*c***) show the difficulty of separating the effects of wind stress and waves in

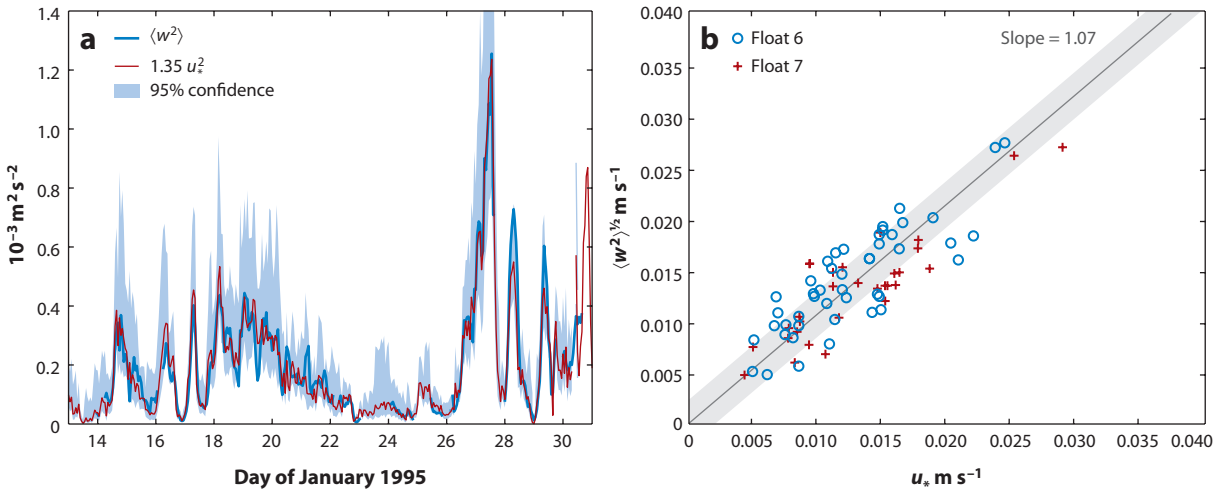

Figure 3

(*a*) Time series of $\langle w^2 \rangle$ (with 95% confidence limits) and $1.35u_*^2$ from the wintertime North Pacific, showing a tight relationship despite rapid changes in both quantities. The values of $\langle w^2 \rangle$ are probably biased high (Harcourt & D'Asaro 2010); a lower limit on the average $\langle w^2 \rangle / u_*^2$ is approximately 1. Adapted from D'Asaro (2001). (*b*) Similar data from a different 36-day record, showing $\langle w^2 \rangle / u_*^2 = 1.07$. Adapted from Tseng & D'Asaro 2004.

long-term open-ocean data. At shorter timescales, winds and waves become less well correlated, with waves growing in response to increasing wind. However, because waves affect the drag coefficient, these short-term effects can be studied only when direct measurements of wind stress are made along with ocean turbulence measurements. Thus, in attempting to explain the unexpectedly tight relationship between wind stress and waves (**Figure 3*a***), D'Asaro (2001) reported that although the correlation between $\langle w^2 \rangle$ and u_*^2 computed indirectly from bulk formulae was sufficiently tight that no additional variance could be explained by adding wave parameters, this did not necessarily imply that waves have no effect.

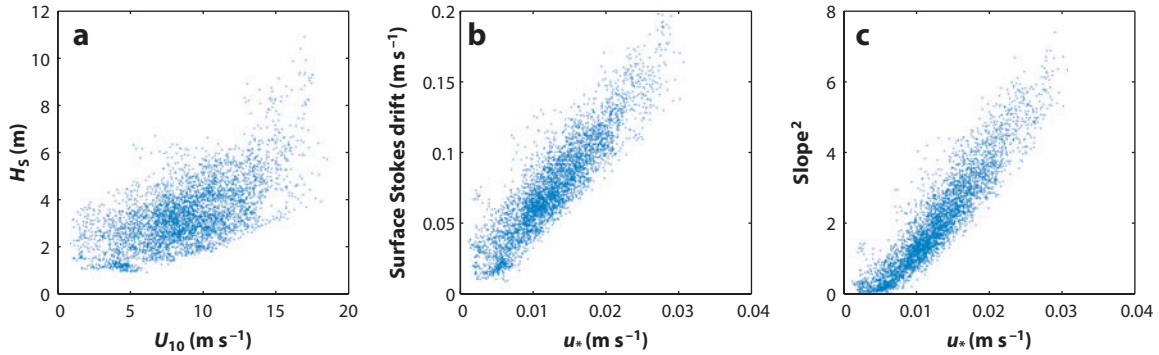

Figure 4

Wind and wave data from ocean station Papa (50°N, 145°W, Coastal Data Information Program station 166; **http://cdip.ucsd.edu**), February–May 2011. (*a*) Significant wave height (H_S) versus 10-m wind speed (U_{10}). (*b*) Surface Stokes drift versus u_*. (*c*) Wave slope squared versus u_*. Wave quantities were computed from resolved spectra measured by a Datawell waverider buoy; u_* was computed from the COARE 2.0 algorithms (Fairall et al. 1996).

6. WAVE BREAKING

A large increase in ε above the classical scaling has been observed repeatedly near the surface and related quantitatively to the loss of energy from surface waves due to breaking (Agrawal et al. 1992, Drennan et al. 1996, Terray et al. 1996). The dissipation resulting from wave breaking is much larger than ε_S, but the profile decays rapidly away from the surface, resuming the classical form below a few significant wave heights from the surface.

Craig & Banner (1994) presented the first of many models including this effect. They modeled wave breaking as an additional input of turbulent kinetic energy at the surface proportional, in their case, to u_*^3. This additional input, added to a conventional second-order turbulent closure model—e.g., Mellor & Yamada's (1982)—produces a turbulent wave boundary layer similar to the observations. The predicted profiles of dissipation and turbulent kinetic energy decay rapidly with depth, so the structure of the boundary layer below this wave layer remains classical. This is thus consistent with **Figure 2*c***, which excludes the upper part of the mixed layer and does not include these wave-breaking effects. This approach increases the turbulence levels in shallow mixed layers, thereby increasing their depths (Noh & Kim 1999) and decreasing the gradients within them (Gerbi et al. 2008), both of which lead to better agreement with observations. More recent studies, including the addition of stochastic wave breaking to LESs of the boundary layer, have been reviewed by Sullivan & McWilliams (2010).

7. LANGMUIR TURBULENCE

Several alternative, nonbreaking energy pathways from surface waves to mixed-layer turbulence have been proposed. Possibly the oldest (Langmuir 1938) and the most well developed is associated with Langmuir circulations, cells, or turbulence. The development of these ideas from conceptual model through hydrodynamic instability and associated laminar models to fully turbulent models has been thoroughly reviewed (Leibovich 1980, Thorpe 2004). Craik & Leibovich (1976) first associated the downwind-aligned surface convergences described by Langmuir (1938) with an instability of the wind-driven boundary layer attributable to the Stokes drift of the surface waves and derived the "CL" (Craik-Leibovich) interaction between the Stokes drift and turbulence that creates this instability. LESs that include this CL interaction, pioneered by Skyllingstad & Denbo (1995) and McWilliams et al. (1997), can create complex representations of the boundary layer driven by the combined effects of wind stress, buoyancy flux, and surface waves. Recent theoretical developments have focused on understanding and parameterizing this Langmuir turbulence; observations have focused on asking how well it represents reality.

The CL interaction introduces a new external parameter, the profile of surface wave Stokes drift $\mathbf{u}^s(z)$, to the buoyancy and momentum fluxes driving Langmuir turbulence. LESs spanning a wide range of nondimensional parameter space are now providing a firmer view of how to parameterize the effect of Stokes drift. McWilliams et al. (1997) proposed a turbulent Langmuir number $La_t = [u_*/u^s(0)]^{1/2}$ as an appropriate nondimensional parameter. However, the Stokes drift profile evaluated from realistic wave spectra using first-order theory decreases rapidly away from the surface, so that the surface value of Stokes drift and thus La_t are sensitive to the details of how the very small waves are represented. For a unidirectional ω^{-4} wave spectrum, for example, the surface Stokes drift is infinite at the surface. Harcourt & D'Asaro (2008) addressed this by focusing on pure wind seas with no surface buoyancy flux and characterized them by a wind speed U_{10} and wave age C_P/U_{10}, where C_P is the phase speed of the peak waves; a fully developed sea has an age of approximately 1.2. They used empirical expressions to consistently include the wave effects on drag and on boundary-layer turbulence over a wide range of winds, wave fields,

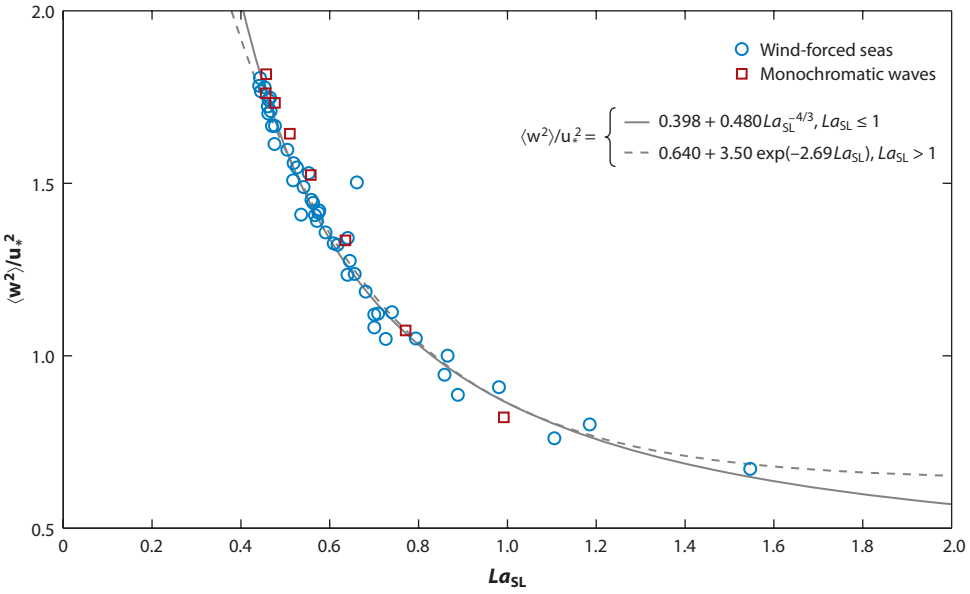

Figure 5

Parameterization of $\langle w^2\rangle/u_*^2$ in Langmuir turbulence from Harcourt & D'Asaro (2008) in terms of the surface-layer Langmuir number La_{SL}. Simulations span a wide range of winds and mixed-layer depths with realistic wind-forced seas (*circles and triangles*) and monochromatic waves (*squares*).

and mixed-layer depths. Harcourt & D'Asaro (2008) introduced a new "surface layer" Langmuir number $La_{\mathrm{SL}} = (u_*/\Delta u^s_{\mathrm{SL}})^{1/2}$, where Δu^s_{SL} is the difference between the Stokes drift averaged over the top 25% of the mixed layer and its value near the base. This formulation removes the strong sensitivity to the surface value. The value of $\langle w^2\rangle/u_*^2$ for all of the simulations could be collapsed to a single function of La_{SL} (**Figure 5**) for both wideband and monochromatic wave fields. However, near the surface, crosswind velocities scale differently from $\langle w^2\rangle/u_*^2$, so this characterization of Langmuir turbulence is still far from complete.

The Harcourt & D'Asaro (2008) formulation shows a strong dependence of $\langle w^2\rangle/u_*^2$ on both La_{t} and, as anticipated by Li et al. (2005), on D_{S}/H, the ratio of the penetration depth of the Stokes drift to the mixed-layer depth. This additional dependence results from the rapid decay of the Stokes drift and its shear, on which the CL forcing depends. The decay is the sum of exponentials from each wave component and is thus faster than exponential. For $D_{\mathrm{S}}/H \geq 1$, the shear is large across the entire layer and forces Langmuir cells spanning the layer. For $D_{\mathrm{S}}/H \ll 1$, the shear is concentrated near the surface and forces only the cells near the surface. Thus, for layer average quantities such as $\langle w^2\rangle/u_*^2$, there is a strong dependence on D_{S}/H. **Figure 6** illustrates this by evaluating the Harcourt & D'Asaro (2008) parameterization for a unidirectional ω^{-4} wave spectrum, cut off at a wavenumber of 1 m^{-1}, over a range of oceanic conditions. The value of $\langle w^2\rangle/u_*^2$ increases monotonically with both La_{SL}^{-2} and D_{S}/H, with the smallest values occurring for small waves and deep mixed layers and the largest values occurring for large waves and shallow mixed layers. For a monotonic spectrum, however, with exponentially decaying Stokes drift, a maximum in $\langle w^2\rangle/u_*^2$ occurs for $D_{\mathrm{S}}/H \approx 1$.

For weak wind and wave forcing (empirically for winds less than approximately 10 m s^{-1}), buoyancy flux can have a large effect. Li et al. (2001) and Belcher et al. (2012) modeled Langmuir

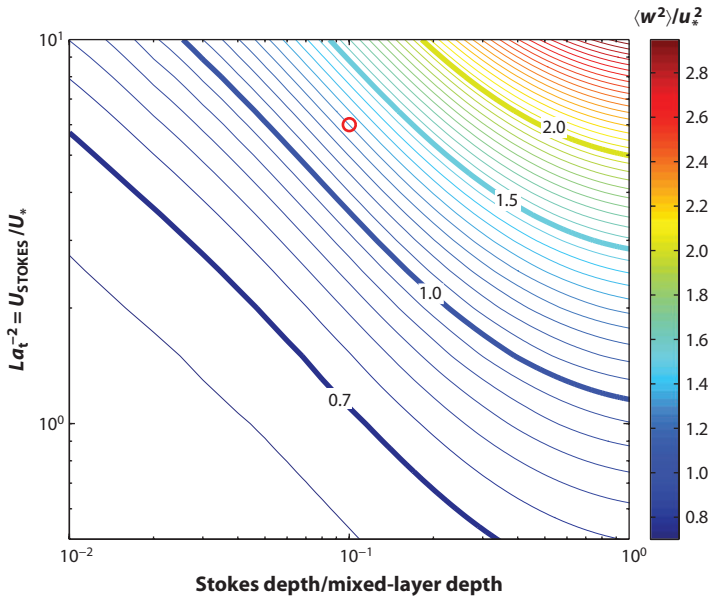

Figure 6

Variations of $\langle w^2 \rangle / u_*^2$ as a function of turbulent Langmuir number La_t, the ratio of surface Stokes drift to wind stress, and the ratio of the Stokes drift penetration $1/e$ depth to the mixed-layer depth using the parameterization of Harcourt & D'Asaro (2008). Contours show the value of $\langle w^2 \rangle / u_*^2$. The calculation assumes a unidirectional ω^{-4} surface wave spectrum aligned with the wind, a directional spreading loss of 0.75 (Webb & Fox-Kemper 2011), and a cutoff wavenumber 24 times the peak wavenumber. The figure spans approximately the range of wind-driven ocean boundary layers; over this range, both effects have roughly equal importance. The red circle is a typical open-ocean condition, as taken from the simulation of Li et al. (2009).

turbulence with buoyancy forcing, and both reported an additional strong dependence on mixed-layer depth, with convection increasingly dominating for deeper mixed layers. Misalignment of wind and waves decreases the wave effects, resulting in a suppression of turbulence for opposing wind and waves. Van Roekel et al. (2012) studied this in detail and improved the directional parameterization of Harcourt and D'Asaro (2008). McWilliams et al. (2012) and Harcourt (2013) attempted to include all of these effects within the context of a unified boundary-layer model.

8. NONBREAKING WAVE TURBULENCE

A second thread of studies has focused on nonbreaking, wave-induced turbulence. Babanin (2006) hypothesized a transition from laminarity to turbulence for the wave-induced motion at a finite Reynolds number based on the wave orbital velocity and wavelength. Because the waves decay with depth, this predicts a turbulence transition in the upper ocean. This is motivated and supported by field observations of turbulence beneath nonbreaking waves and of strong Reynolds stresses beneath waves (Cavaleri & Zecchetto 1987), by laboratory measurements of strong turbulence beneath nonbreaking waves (Babanin & Haus 2009, Dai et al. 2010), and by the improvement in global model performance when additional mixing is included in the boundary-layer parameterization (Huang et al. 2012). Quantification of this effect (Huang & Qiao 2010, Qiao et al. 2004) relies on mixing length arguments to specify a viscosity $\sim l^2 S$, where the mixing length l is taken as

the wave particle displacement and the shear S is taken as vertical wave shear; it thereby assumes that the displacements of the surface wave field can be modeled as a random walk with the time and space scales of the waves.

The validity of these arguments has come under serious scrutiny in the literature. A turbulent transition for surface waves and its parameterization by an eddy viscosity run contrary to the "conventional understanding that irrotational wave theories provide a good approximation of non-wind-forced wave behavior" (Beyá et al. 2012). The results of Cavaleri & Zecchetto (1987) have been attributed to "surface waves reflecting off the observation platform" (Santala 1991) and "small uncertainties in sensor orientation" (Gerbi et al. 2008, Trowbridge 1998). Similar measurements carried out by Gerbi et al. (2008) show no similar large stresses. The laboratory results of Babanin & Haus (2009) could not be replicated by Beyá et al. (2012) and (quoting the latter) run contrary to many "laboratory wave experiments. . .carried out in the early 1960s. . .[in which] no evidence of turbulence was reported, and steep waves behaved as predicted by the high order irrotational wave theories within the accuracy of the theories and experimental techniques at the time." Furthermore, the hypothesis of a turbulent wave transition has not been verified by demonstrations of a hydrodynamic instability of the waves that might be responsible for this transition nor by simulations of the equations of motion showing the finite amplitude evolution of such an instability. Finally, field observations of turbulence beneath nonbreaking waves can be explained easily by alternative sources of this turbulence, such as surface buoyancy flux and shear instability, and enhanced boundary-layer turbulence on a global scale can be explained by wave breaking and Langmuir turbulence.

9. OBSERVATIONS OF LANGMUIR TURBULENCE

Although observations of mixed-layer turbulence are difficult, the predictive capabilities of LES models and the limited available observations are beginning to allow quantitative testing of Langmuir turbulence theories. Kukulka et al. (2009) used an LES model of Langmuir turbulence without wave breaking to simulate open-ocean sonar observations of near-surface bubble clouds made during a 1990 FLIP experiment (Smith 1992). Simulations that include the CL wave interactions predict the observed crosswind velocity variance well, whereas those that do not include these interactions are low by 30–50% (**Figure 7**). Similarly, mixed-layer deepening approximately matches the observations with waves but is approximately half that observed without waves.

Lien et al. (2008) measured Langmuir circulations in a shallow (1–2-m) boundary layer in a strongly stratified estuary with short fetch and thus small surface waves. Although near-surface convergences were clearly present (as measured by the aggregation of floating popcorn), the energy input by the CL vortex terms (as measured directly from vorticity and velocity) was smaller than the direct input from the wind. LES runs both with and without Stokes drift produced surface convergence streaks and vertical profiles of dissipation rate, vorticity, and velocity consistent with the observations. These observations and model results challenge the traditional view that the surface convergences usually associated with Langmuir circulations must result from the CL wave interaction. Nevertheless, they support the validity of LESs of upper-ocean turbulence, albeit in a case where the CL effects are weak.

The most detailed comparisons of Langmuir turbulence data and theory have been made using data from shallow-water (∼15 m) environments, where long time series of all three components of velocity are available. Measurements have been reported from the Martha's Vineyard (Kukulka et al. 2012) and LEO-15 (Gargett & Wells 2007, Gargett et al. 2004, Tejada-Martínez & Grosch 2007) observatories. LESs are again consistent with the data only when the CL force is included in the models (**Figure 8**). In particular, the detailed observations of Gargett & Wells

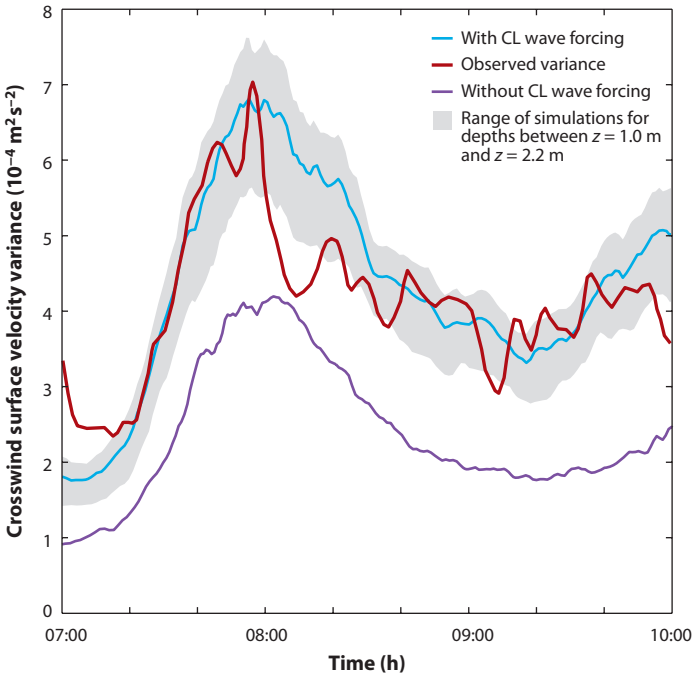

Figure 7

Comparison of large-eddy simulations of Langmuir turbulence with observations by Smith (1992). Observed near-surface crosswind velocity variance matches simulations at 1.4-m depth with CL (Craik-Leibovich) wave forcing much better than it does simulations without CL wave forcing. The gray area indicates the range of simulation results between depths of 1.0 m and 2.2 m, corresponding roughly to the instrumental depth response. Adapted from Kukulka et al. (2009).

(2007) demonstrated the dramatic change in polarization of the turbulent eddies predicted by theory. For shear-driven turbulence without the CL force, velocity fluctuations are dominantly downwind, with much weaker vertical and crosswind components. Under strong CL forcing, the vertical and crosswind components become much stronger, consistent with the qualitative view of coherent Langmuir cells aligned downwind and circulating fluid in a vertical/crosswind plane. These eddies are more effective at vertical mixing and therefore reduce the gradients within the mixed layer (Gerbi et al. 2008). In shallow water, this prediction is modified near the bottom by the intensification of the downwind velocity fluctuations, as is also observed in the data.

10. PERSPECTIVE

Observations now show that the upper-ocean boundary layer differs fundamentally from the classical laboratory and atmospheric boundary layer owing to the influence of surface waves. The differences appear in at least two ways. First, wave breaking produces a layer of intense turbulence near the surface, with dissipation rates much higher than those in the classical model. This has been known for many years and continues to be verified. Second, and more recently, measurements below the wave-breaking layer show significant deviations from the classical model in the form of the turbulence, consistent with the predictions of LES models of Langmuir turbulence driven by the Stokes drift of the waves. The resulting turbulent eddies are more coherent, have a larger vertical velocity, and mix more effectively.

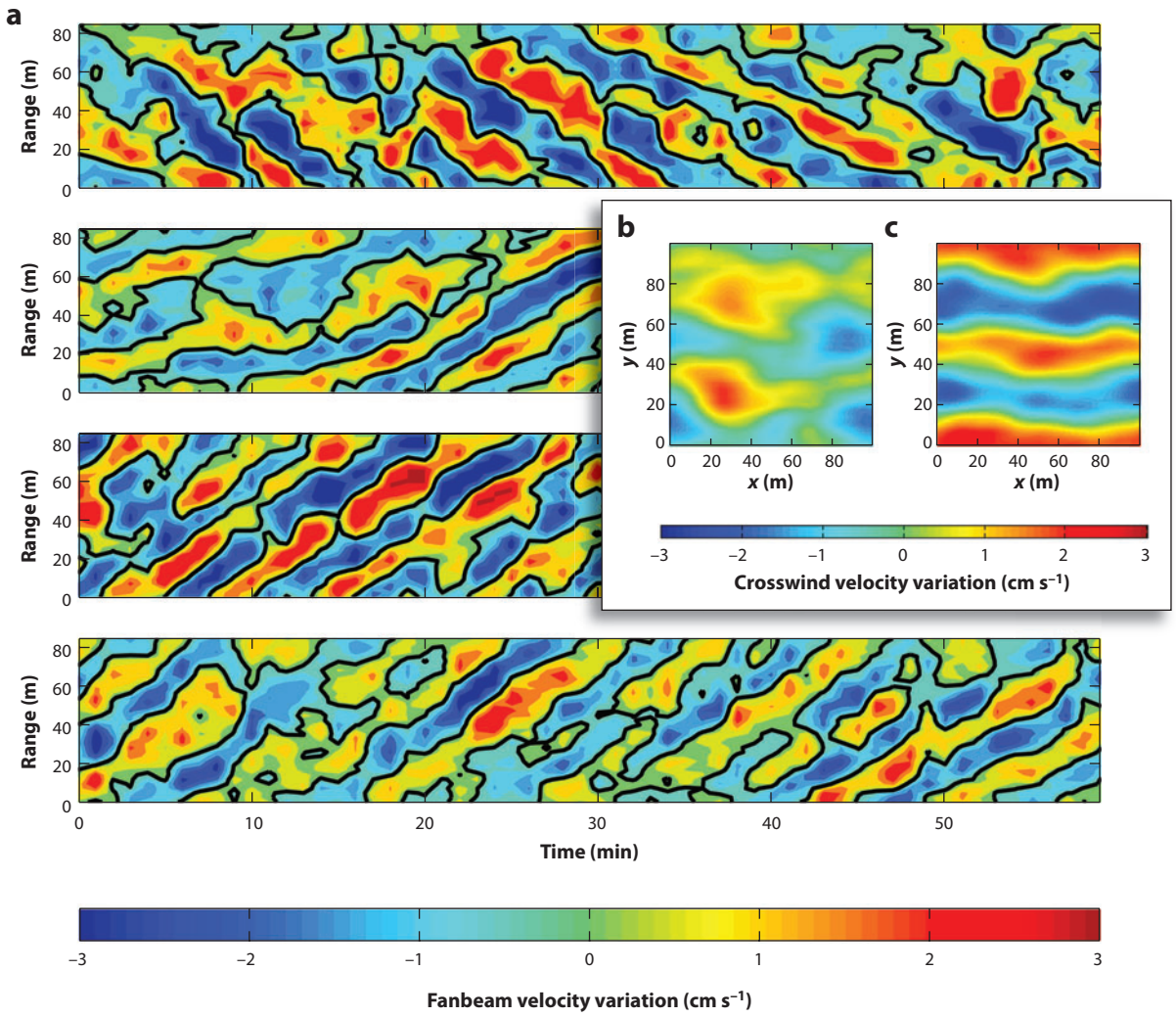

Figure 8

Comparison of large-eddy simulations of Langmuir turbulence with observed patterns of near-surface crosswind velocity in 16-m water depth. (*a*) Selected observations of crosswind velocity, showing stripes of alternating sign. (*b*) Large-eddy simulations without CL (Craik-Leibovich) wave forcing, showing weaker stripes compared with the observations. (*c*) Large-eddy simulations with CL wave forcing, which are closer to observed patterns and amplitude. Adapted from Kukulka et al. (2012).

Many aspects of surface wave interactions with the ocean boundary layer require further exploration. Gemmrich (2012) reported strong effects of bubble buoyancy on the turbulence. Teixeira (2012) and colleagues argued for the strong effects of wave straining on the turbulent cascade near the surface. All current approaches mathematically flatten the ocean surface, thereby ignoring its geometrical complexity. Thus, although the existing observations support the hypothesis that Langmuir turbulence—driven by air–sea fluxes of momentum, heat, and moisture and the profile of surface wave Stokes drift, and modified by surface wave breaking—describes the upper-ocean boundary layer, the data available are very limited, especially from the open ocean. In particular,

we do not know when, where, or how Langmuir turbulence becomes a poor representation of the boundary-layer turbulence.

DISCLOSURE STATEMENT

The author is not aware of any affiliations, memberships, funding, or financial holdings that might be perceived as affecting the objectivity of this review.

ACKNOWLEDGMENTS

The author acknowledges numerous grants from the National Science Foundation and Office of Naval Research over many decades supporting work in this area. This particular review was inspired by and partially supported by an NSF Collaboration in Mathematical Geosciences Collaborative Research Grant (OCE-0934580).

LITERATURE CITED

Agrawal YC, Terray EA, Donelan MA, Hwang PA, Williams AJ III, et al. 1992. Enhanced dissipation of kinetic energy beneath surface waves. *Nature* 359:219–20

Babanin AV. 2006. On a wave-induced turbulence and a wave-mixed upper ocean layer. *Geophys. Res. Lett.* 33:L20605

Babanin AV, Haus BK. 2009. On the existence of water turbulence induced by nonbreaking surface waves. *J. Phys. Oceanogr.* 39:2675–79

Belcher SE, Grant ALM, Hanley KE, Fox-Kemper B, Van Roekel L, et al. 2012. A global perspective on Langmuir turbulence in the ocean surface boundary layer. *Geophys. Res. Lett.* 39:L18605

Beyá JF, Peirson WL, Banner ML. 2012. Turbulence beneath finite amplitude water waves. *Exp. Fluids* 52:1319–30

Cantwell B. 1981. Organized motion in turbulent flow. *Annu. Rev. Fluid Mech.* 13:457–515

Carniel S, Kantha LH, Book JW, Sclavo M, Prandke H. 2012. Turbulence variability in the upper layers of the Southern Adriatic Sea under a variety of atmospheric forcing conditions. *Cont. Shelf Res.* 44:39–56

Cavaleri L, Zecchetto S. 1987. Reynolds stresses under wind waves. *J. Geophys. Res.* 92:3894–904

Craig PD, Banner ML. 1994. Modeling wave-enhanced turbulence in the ocean surface layer. *J. Phys. Oceanogr.* 24:2546–59

Craik ADD, Leibovich S. 1976. A rational model for Langmuir circulations. *J. Fluid Mech.* 73:401–26

Dai D, Qiao F, Sulisz W, Han L, Babanin A. 2010. An experiment on the nonbreaking surface-wave-induced vertical mixing. *J. Phys. Oceanogr.* 40:2180–88

D'Asaro EA. 1978. Mixed layer velocities induced by internal waves. *J. Geophys. Res.* 83:2437–38

D'Asaro EA. 2001. Turbulent vertical kinetic energy in the ocean mixed layer. *J. Phys. Oceanogr.* 31:3530–37

D'Asaro EA. 2003. Performance of autonomous Lagrangian floats. *J. Atmos. Ocean. Technol.* 20:896–911

D'Asaro EA. 2004. Air-sea heat flux measurements from nearly neutrally buoyant floats. *J. Atmos. Ocean. Technol.* 21:1086–94

D'Asaro EA, Farmer DM, Osse JT, Dairiki GT. 1996. A Lagrangian float. *J. Atmos. Ocean. Technol.* 13:1230–46

Drennan WM, Donelan MA, Terray EA, Katsaros KB. 1996. Oceanic turbulence dissipation measurements in SWADE. *J. Phys. Oceanogr.* 26:808–15

Fairall CW, Bradley EF, Rogers DP, Edson JB, Young GS. 1996. Bulk parameterization of air–sea fluxes in TOGA COARE. *J. Geophys. Res.* 101:3747–67

Fox-Kemper B, Danabasoglu G, Ferrari R, Griffies SM, Hallberg RW, et al. 2011. Parameterization of mixed layer eddies. III. Implementation and impact in global ocean climate simulations. *Ocean Model.* 39:61–78

Gargett AE, Wells JR. 2007. Langmuir turbulence in shallow water. Part 1. Observations. *J. Fluid Mech.* 576:27–61

Gargett AE, Wells JR, Tejada-Martínez AE, Grosch CE. 2004. Langmuir supercells: a mechanism for sediment resuspension and transport in shallow seas. *Science* 306:1925–28

Gemmrich J. 2012. Bubble-induced turbulence suppression in Langmuir circulation. *Geophys. Res. Lett.* 39:L10604

Gerbi GP, Trowbridge JH, Edson JB, Plueddemann AJ, Terray EA, Fredericks JI. 2008. Measurements of momentum and heat transfer across the air-sea interface. *J. Phys. Oceanogr.* 38:1054–72

Gerbi GP, Trowbridge JH, Terray EA, Plueddemann AJ, Kukulka T. 2009. Observations of turbulence in the ocean surface boundary layer: energetics and transport. *J. Phys. Oceanogr.* 39:1077–96

Gregg MC. 1998. Estimation and geography of diapycnal mixing in the stratified ocean. *Coast. Estuar. Stud.* 54:305–38

Harcourt RR. 2013. A second moment closure model of Langmuir turbulence. *J. Phys. Oceanogr.* 43:673–97

Harcourt RR, D'Asaro EA. 2008. Large-eddy simulation of Langmuir turbulence in pure wind seas. *J. Phys. Oceanogr.* 38:1542–62

Harcourt RR, D'Asaro EA. 2010. Measurement of vertical kinetic energy and vertical velocity skewness in oceanic boundary layers by imperfectly Lagrangian floats. *J. Atmos. Ocean. Technol.* 27:1918–35

Harcourt RR, Steffen EL, Garwood RW, D'Asaro EA. 2002. Fully Lagrangian floats in Labrador Sea deep convection: comparison of numerical and experimental results. *J. Phys. Oceanogr.* 32:493–510

Huang CJ, Qiao F. 2010. Wave-turbulence interaction and its induced mixing in the upper ocean. *J. Geophys. Res.* 115:C04026

Huang CJ, Qiao F, Shu Q, Song Z. 2012. Evaluating austral summer mixed-layer response to surface wave-induced mixing in the Southern Ocean. *J. Geophys. Res.* 117:C00J18

Kukulka T, Plueddemann AJ, Sullivan PP. 2012. Nonlocal transport due to Langmuir circulation in a coastal ocean. *J. Geophys. Res.* 117:C12007

Kukulka T, Plueddemann AJ, Trowbridge JH, Sullivan PP. 2009. Significance of Langmuir circulation in upper ocean mixing: comparison of observations and simulations. *Geophys. Res. Lett.* 36:L10603

Langmuir I. 1938. Surface motion of water induced by wind. *Science* 87:119–23

Leibovich S. 1980. On wave-current interaction theories of Langmuir circulations. *J. Fluid Mech.* 99:715–24

Li M, Garrett C, Skyllingstad E. 2005. A regime diagram for classifying turbulent large eddies in the upper ocean. *Deep-Sea Res. I* 52:259–78

Li M, Vagle S, Farmer DM. 2009. Large eddy simulations of upper-ocean response to a midlatitude storm and comparison with observations. *J. Phys. Oceanogr.* 39:2295–309

Li X, Chao Y, McWilliams JC, Fu L-L. 2001. A comparison of two vertical-mixing schemes in a Pacific Ocean general circulation model. *J. Clim.* 14:1377–98

Lien R-C, Sanford TB, Tsai W-T. 2008. Observations of turbulence mixing and vorticity in a littoral surface boundary layer. *J. Phys. Oceangr.* 38:648–69

Lombardo CP, Gregg MC. 1989. Similarity scaling of viscous and thermal dissipation in a convecting surface boundary layer. *J. Geophys. Res.* 94:6273–84

McPhee MG, Smith JD. 1976. Measurements of the turbulent boundary layer under pack ice. *J. Phys. Oceanogr.* 6:696–711

McWilliams JC, Huckle E, Liang J-H. 2012. The wavy Ekman layer: Langmuir circulations, breaking waves, and Reynolds stress. *J. Phys. Oceanogr.* 42:1793–816

McWilliams JC, Sullivan PP, Moeng C-H. 1997. Langmuir turbulence in the ocean. *J. Fluid Mech.* 334:1–30

Mellor GL, Yamada T. 1982. Development of a turbulence closure model for geophysical fluid problems. *Rev. Geophys. Space Phys.* 20:851–75

Munk WH. 1981. Internal waves and small-scale processes. In *Evolution of Physical Oceanography: Scientific Surveys in Honor of Henry Stommel*, ed. BA Warren, C Wunsch, pp. 264–91. Cambridge, MA: MIT Press

Noh Y, Kim HJ. 1999. Simulations of temperature and turbulence structure of the oceanic boundary layer with the improved near-surface process. *J. Geophys. Res.* 104:15621–634

Pollard RT, Millard RC. 1970. Comparison between observed and simulated wind-generated inertial oscillations. *Deep-Sea Res. Oceanogr. Abstr.* 17:813–21

Qiao F, Yuan Y, Yang Y, Zheng Q, Xia C, Ma J. 2004. Wave-induced mixing in the upper ocean: distribution and application to a global ocean circulation model. *Geophys. Res. Lett.* 31:L11303

Sallée JB, Shuckburgh E, Bruneau N, Meijers AJS, Bracegirdle TJ, Wang Z. 2013a. Assessment of Southern Ocean mixed-layer depths in CMIP5 models: historical bias and forcing response. *J. Geophys. Res.* 118:1845–62

Sallée JB, Shuckburgh E, Bruneau N, Meijers AJS, Bracegirdle TJ, et al. 2013b. Assessment of Southern Ocean water mass circulation and characteristics in CMIP5 models: historical bias and forcing response. *J. Geophys. Res.* 118:1830–44

Santala MJ. 1991. *Surface-referenced current meter measurements*. PhD thesis. Woods Hole Oceanogr. Inst., Woods Hole, MA, and Mass. Inst. Technol., Cambridge, MA (Joint Program in Oceanography)

Shay TJ, Gregg MC. 1986. Convectively driven turbulent mixing in the upper ocean. *J. Phys. Oceanogr.* 16:1777–98

Skyllingstad ED, Denbo DW. 1995. An ocean large-eddy simulation of Langmuir circulations and convection in the surface mixed layer. *J. Geophys. Res.* 100:8501–22

Smith JA. 1989. Doppler sonar and surface waves: range and resolution. *J. Atmos. Ocean. Technol.* 6:680–96

Smith JA. 1992. Observed growth of Langmuir circulation. *J. Geophys. Res.* 97:5651–64

Steffen EL, D'Asaro EA. 2002. Deep convection in the Labrador Sea as observed by Lagrangian floats. *J. Phys. Oceanogr.* 32:475–92

Sullivan PP, McWilliams JC. 2010. Dynamics of winds and currents coupled to surface waves. *Annu. Rev. Fluid Mech.* 42:19–42

Teixeira MAC. 2012. The influence of Langmuir turbulence on the scaling for the dissipation rate in the oceanic boundary layer. *J. Geophys. Res.* 117:C05015

Tejada-Martínez AE, Grosch CE. 2007. Langmuir turbulence in shallow water. Part 2. Large-eddy simulation. *J. Fluid Mech.* 576:63–108

Terray EA, Donelan MA, Agrawal YC, Drennan WM, Kahma KK, et al. 1996. Estimates of kinetic energy dissipation under breaking waves. *J. Phys. Oceanogr.* 26:792–807

Thomson J, Gemmrich JR, Jessup AT. 2009. Energy dissipation and the spectral distribution of whitecaps. *Geophys. Res. Lett.* 36:L11601

Thorpe SA. 2004. Langmuir circulation. *Annu. Rev. Fluid Mech.* 36:55–79

Trowbridge JH. 1998. On a technique for measurement of turbulent shear stress in the presence of surface waves. *J. Atmos. Ocean. Technol.* 15:290–98

Tseng R-S, D'Asaro EA. 2004. Measurements of turbulent vertical kinetic energy in the ocean mixed layer from Lagrangian floats. *J. Phys. Oceanogr.* 34:1984–90

Umlauf L, Burchard H. 2005. Second-order turbulence closure models for geophysical boundary layers: a review of recent work. *Cont. Shelf Res.* 25:795–827

Van Roekel LP, Fox-Kemper B, Sullivan PP, Hamlington PE, Haney SR. 2012. The form and orientation of Langmuir cells for misaligned winds and waves. *J. Geophys. Res.* 117:C05001

Vermeulen B, Hoitink AJF, Sassi MG. 2011. Coupled ADCPs can yield complete Reynolds stress tensor profiles in geophysical surface flows. *Geophys. Res. Lett.* 38:L06406

Webb A, Fox-Kemper B. 2011. Wave spectral moments and Stokes drift estimation. *Ocean Model.* 40:273–88

Weller RA, Price JF. 1988. Langmuir circulation within the oceanic mixed layer. *Deep-Sea Res. A* 35:711–47

Zedel L, Farmer D. 1991. Organizing structures in subsurface bubble clouds: Langmuir circulation in the open ocean. *J. Geophys. Res.* 96:8889–900